X-ray observations of the nova shell IPHASX J210204.7+471015

J. A. Toalá [1]⋆ G. Rubio [2,3] E. Santamaría [2,3] M. A. Guerrero [4] S. Estrada-Dorado,[1]
G. Ramos-Larios [2,3] and L. Sabin [5]

[1]*Instituto de Radioastronomía y Astrofísica (IRyA), UNAM Campus Morelia, Apartado Postal 3-72, 58090 Morelia, Mexico*
[2]*CUCEI, Universidad de Guadalajara, Blvd. Marcelino García Barragán 1421, 44430 Guadalajara, Jalisco, Mexico*
[3]*Instituto de Astronomía y Meteorología, Dpto. de Física, CUCEI, Av. Vallarta 2602, 44130 Guadalajara, Jalisco, Mexico*
[4]*Instituto de Astrofísica de Andalucía, IAA-CSIC, Glorieta de la Astronomía s/n, E-18008 Granada, Spain*
[5]*Instituto de Astronomía, Universidad Nacional Autonoma de México, Apartado Postal 877, 22800 Ensenada, Baja California, Mexico*

ABSTRACT

We present the analysis of *XMM–Newton* European Photon Imaging Camera (EPIC) observations of the nova shell IPHASX J210204.7+471015. We detect X-ray emission from the progenitor binary star with properties that resemble those of underluminous intermediate polars such as DQ Herculis (DQ Her): an X-ray-emitting plasma with temperature of $T_X = (6.4 \pm 3.1) \times 10^6$ K, a non-thermal X-ray component, and an estimated X-ray luminosity of $L_X = 10^{30}$ erg s^{-1}. Time series analyses unveil the presence of two periods, the dominant with a period of 2.9 ± 0.2 h, which might be attributed to the spin of the white dwarf, and a secondary of 4.5 ± 0.6 h that is in line with the orbital period of the binary system derived from optical observations. We do not detect extended X-ray emission as in other nova shells probably due to its relatively old age (130–170 yr) or to its asymmetric disrupted morphology that is suggestive of explosion scenarios different to the symmetric ones assumed in available numerical simulations of nova explosions.

Key words: binaries: general – stars: evolution – novae, cataclysmic variables – X-rays: individual: IPHASX J 210204.7+471015 – X-rays: stars – transients: novae.

1 INTRODUCTION

Nova events are the result of thermonuclear explosions from binary systems that occur when a white dwarf (WD) accretes H-rich material from a companion (e.g. Gallagher & Starrfield 1978). Because of momentum conservation, the material forms an accretion disc before being accreted by the WD. The material in the disc spirals down on to the WD while it's being heated up by friction. If the accretion rate on to the WD is low, the accreted material becomes degenerate, making the pressure and temperature to increase dramatically. An explosion will ignite the material accreted on the surface of the WD through a thermonuclear runaway event – a nova explosion. This thermonuclear runaway releases and initial energy $E_0 \sim 10^{44}$–10^{45} erg, ejecting $M_{ej} \approx 10^{-5}$–10^{-4} M$_\odot$ at velocities as high as $v_{ej} \gtrsim 10^3$ km s^{-1} (see e.g. Bode 2010; Della Valle & Izzo 2020) into the interstellar medium (ISM).

The violent ejection of material in the nova event sweeps, shocks, and compresses the surrounding ISM. This interaction will create an adiabatic shock that heats up the gas inside the nova remnant creating a hot bubble similarly to that of supernovae (SNe) and wind-blown bubbles (Güdel et al. 2008). The post-shock temperature of this hot bubble can be estimated as $T \propto v_{ej}^2$ (Dyson & Williams 1997). The highly supersonic ejecta should produce post-shock temperatures

in excess to 10^6 K that in principle could be detected with X-ray instruments. Because of the high thermal energy of the hot bubble, it will dominate the dynamical evolution of the nova remnant until its dispersal into the ISM. During its evolution, the nova shell will experience Rayleigh–Taylor instabilities and will be disrupted (see e.g. Orlando, Drake & Miceli 2017); a characteristic that is evident in narrow-band imaging of novae shells (see Santamaría et al. 2020, and references therein). The clumps and filaments will create ablation flows (e.g. Vaytet, O'Brien & Rushton 2007), mixing the nova shell material with that of the hot bubble, reducing its temperature to $\sim 10^6$ K enhancing the production of soft X-ray emission (Toalá & Arthur 2018).

There are two nova remnants with unambiguously resolved extended X-ray emission and they seem to exhibit contrasting aspects of the same event. On one hand, GK Persei (GK Per) can be described as a scaled-down version of a SN remnant producing its thermal and non-thermal X-ray emission as the result of the expansion of the shock wave compressing the surrounding ISM (Balman & Ögelman 1999; Balman 2005; Takei et al. 2015; Yuasa, Hayashi & Ishida 2016). Meanwhile DQ Herculis (DQ Her) has been recently suggested to harbour the first ever detected magnetized jet disclosing more fundamental physics acting at the level of the progenitor binary star (Toalá et al. 2020).

Extended X-ray emission has been suggested to be present in other nova-like systems: the classical nova RR Pic (Balman & Küpcü-Yoldaş 2004), the cataclysmic variable (CV) DK Lac (Takei,
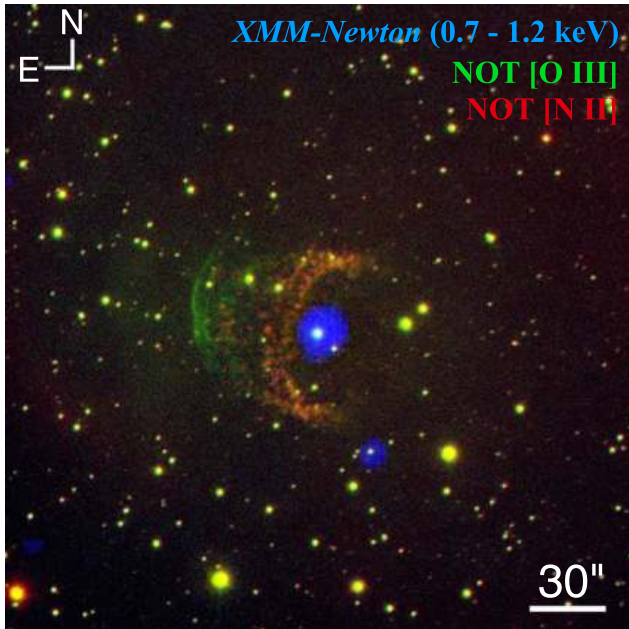
⋆ E-mail: j.toala@irya.unam.mx

Figure 1. Optical and X-ray colour-composite picture of IPHASX J 210204.7+471015. Red and green correspond to narrow-band images obtained with the Nordic Optical Telescope (NOT; see Guerrero et al. 2018), while blue corresponds to the *XMM–Newton* X-ray image in the 0.7–1.2 keV energy range. The progenitor star system is at the centre of the image. North is up, east to the left.

Sakamoto & Drake 2013), and those around the recurrent novae T Pyx (Balman 2014) and RS Oph (Luna et al. 2009). However, their marginal detections, in some cases unresolved, make it difficult to unveil the true spatial distribution of the X-ray emission.

In contrast, X-ray emission from the central binary system is often reported in the literature. The evolution of the X-ray properties of the binary system in a nova eruption vary significantly during the outburst and post-outburst (see e.g. Singh et al. 2021, and references therein). In the non-magnetic cases, after accretion is re-established, the progenitor system will behave similarly to a CV (Hernanz & Sala 2002, 2010; Sala et al. 2017). Their X-ray emission is likely to be produced on post-shock regions at the base of the accreting surface on the WD (Eracleous, Halpern & Patterson 1991; Baskill, Wheatley & Osborne 2005). In the cases in which the WD has a strong magnetic field ($B \approx 1$–10 MG), as the case of the so-called intermediate polars (IPs), it quenches the inner region of the accretion disc at the magnetospheric radius of the WD. The material falls into the WD following the magnetic field lines towards the polar regions forming a shock (see Patterson 1994) and producing X-rays (see Worpel et al. 2020, and references therein). In such cases the spin of the WD is not synchronized to the orbit of the binary system, and thus, some X-ray variability is seen even in quiescent state (e.g. Mukai, Still & Ringwald 2003).

In this paper, we present an X-ray characterization of the nova shell IPHASX J210204.7+471015 (hereinafter J210204; see Fig. 1) and its progenitor system. J210204 was discovered as part of the Isaac Newton Telescope Photometric Hα Survey (IPHAS; Drew et al. 2005; Barentsen et al. 2014) and proposed to be a possible planetary nebula (Sabin et al. 2014), but later characterized as a nova shell (Guerrero et al. 2018). The most obvious structure of J210204 illustrated in Fig. 1 is a clumpy incomplete ring-like structure mainly detected in [N II], with most of the knots exhibiting a cometary

morphology. This ring-like structure lacks emission towards the west with less dense fewer knots. A different structure is detected in [O III], a bow-shock-like feature towards the east, which might be caused as the shock wave expands into the ISM. The clear asymmetric morphology of J210204, reminiscent of the classical nova AT Cnc (Shara et al. 2012), is not common for nova shells. Their morphology represents the best piece of evidence of asymmetric explosions shaping novae shells.

We use *XMM–Newton* to search and characterize the X-ray emission from its central engine and to assess the presence of a hot bubble. This paper is organized as follows. In Section 2, we present the observations and the data analysis. In Section 3, we present our results. A discussion is presented in Section 4. Finally, we summarize our results in Section 5.

2 OBSERVATIONS AND DATA PREPARATION

J210204 was observed with the three European Photon Imaging Cameras (EPICs) on-board *XMM–Newton* during 2020 May 5 for a total observation time of 72 ks (Obs. ID: 0863070101; PI: M. A. Guerrero). The observations were obtained on the Extended Full Frame mode for the pn camera and in the Full Frame mode for the MOS1 and MOS2 cameras. All observations were obtained with the medium optical blocking filter. The total exposure times on the MOS1, MOS2, and pn cameras are 67.9, 68.1, and 64.7 ks, respectively.

The observation data files (ODF) were processed with the Science Analysis System (SAS) version 19.0.[1] The event files were produced using the *epproc* and *emproc* SAS tasks with the calibration files obtained on 2020 November 30. In order to excise periods of high background we created EPIC light curves binning the data over 100 s for the 10–12 keV energy range. The background was considered high for count rates of 0.2 counts s^{-1} for the EPIC-MOS and 0.45 counts s^{-1} for EPIC-pn. After excising bad periods of time, the net exposures times for the MOS1, MOS2, and pn cameras resulted in 58.2, 57.9, and 40.8 ks, respectively.

The clean event files of the three EPIC cameras have been combined using the *merge* SAS task only for purposes of illustration. In Fig. 2, we show this image and the position of the progenitor star of J210204. The central source is detected in X-rays.

In order to extract spectra of J210204, we defined a source circular aperture with a radius of 20 arcsec and a background aperture from a region with no contribution from point sources in the vicinity of J210204. The resultant count rates for the central star of J210204 obtained from the MOS1, MOS2, and pn cameras are 0.70 ± 0.15, 0.60 ± 0.17, and 3.7 ± 0.4 counts ks^{-1} with total detected count numbers of 40 ± 9, 32 ± 9, and 150 ± 16 counts for the MOS1, MOS2, and pn cameras, respectively. The background-subtracted EPIC-pn spectrum is presented in Fig. 3. We do not show the MOS spectra because their low count rates result in a limited quality.

To further search for extended X-ray emission filling the nebular shell of J210204, we also analysed the data following the Extended Source Analysis Software (ESAS) tasks (Snowden, Collier & Kuntz 2004; Kuntz & Snowden 2008; Snowden et al. 2008), which are currently included as part of SAS. The ESAS tasks apply more restrictive event rejection criteria, cleaning the data for the possible contamination from the astrophysical background, the soft proton background, and solar wind charge-exchange reactions, which have important contributions at energies <1.5 keV. Independent pn,
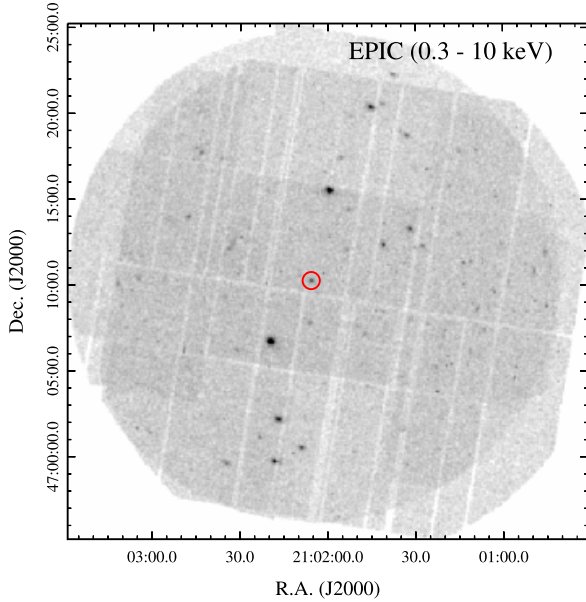
---

[1] https://www.cosmos.esa.int/web/xmm-newton/what-is-sas

Figure 2. *XMM–Newton* EPIC (MOS1+MOS2+pn) image in the 0.3–10 keV energy range of IPHASX J 210204.7+471015 (J210204). The position of the progenitor star of J210204 is shown with a red circle with an angular radius of 20 arcsec.
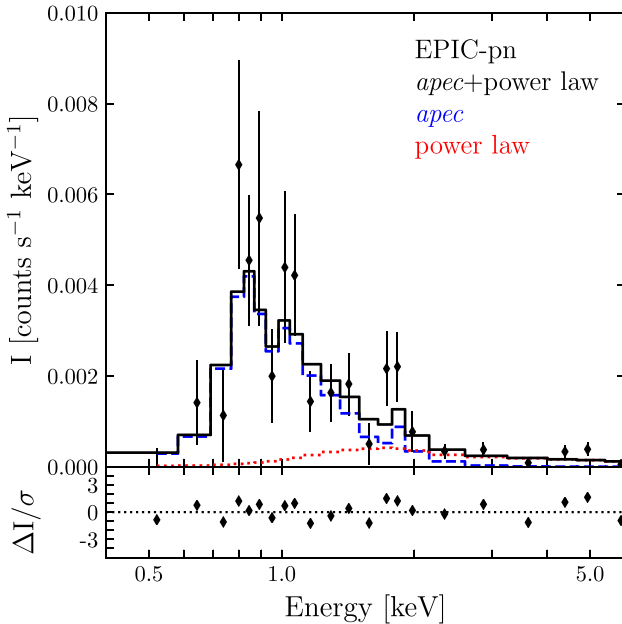

Figure 3. Background-subtracted EPIC-pn spectrum of the central source in J210204 (black diamonds). The solid black line represents the total model, whilst the dashed (blue) and dotted (red) lines show the contribution from the *apec* and power-law components. The spectrum has been extracted requesting a minimum of 10 counts per spectral bin. The bottom panel presents the residuals of the best-fitting model.

MOS1, and MOS2 images were extracted, merged together, and corrected for exposure maps. This was done for three different energy ranges, namely, a soft (0.3–0.7 keV), a medium (0.7–1.2 keV), and a hard (1.2–5.0 keV) band.

No extended X-ray emission was detected in any of the three EPIC images produced with the ESAS tasks, but only the presence of point sources in the vicinity of J210204. In Fig. 1, we compare the medium X-ray band with optical images obtained at the Nordic Optical Telescope (NOT) taken with [O III] and [N II] narrow band filters.

3 ANALYSIS AND RESULTS

The bulk of the emission in the EPIC-pn spectrum of the central source of J210204 is in the energy range between 0.4 and 2 keV (see Fig. 3). The spectrum hints at the presence of three emission lines at $\sim$0.8, $\sim$1.0, and $\sim$1.8 keV. The first two might be attributed to Ne IX and Ne X emission lines, respectively, whilst the latter might be due to Si XIII emission lines. We note that a certain energetic continuum can be seen in the spectrum from 2.0 to 6.0 keV.

In order to estimate its physical properties, the EPIC-pn spectrum of the central star of J210204 was modelled using the X-Ray Spectral Fitting Package (XSPEC; Arnaud 1996) version 12.9.1. A first model was attempted by accounting for a single optically thin *apec* plasma emission model. This single-component model reproduced the soft part of the spectrum, but it is notably deficient for the hard X-ray emission above 2.0 keV. Models with two components were subsequently attempted.

Our first model included two *apec* plasma components with solar abundances (Wilms, Allen & McCray 2000) that resulted in a relatively good fit with a reduced χ^2 of 1.22. The soft component has a plasma temperature of $kT_1 = 0.52^{+0.24}_{-0.27}$ keV and was fitted with a hydrogen column density $N_{\mathrm{H}} = (8.0^{+2.7}_{-3.6}) \times 10^{21}$ cm^{-2}. The latter is consistent with the extinction measured in optical spectra (see Guerrero et al. 2018). However, XSPEC had troubles fitting the second component, resulting in an undefined plasma temperature kT_2 between 2 and 64 keV.

A better fit to the EPIC-pn spectrum was achieved by a temperature plasma emission model plus a power-law component. This fit resulted in a similar reduced χ^2 of 1.20, a column density $N_{\mathrm{H}} = (8.1^{+2.5}_{-3.4}) \times 10^{21}$ cm^{-2}, and a plasma component with $kT_1 = 0.55^{+0.22}_{-0.27}$ keV. The power-law component is characterized by a photon index $\Gamma = 1.0^{+1.0}_{-1.4}$. The XSPEC normalization parameters[2] of the two components are $A_{\mathrm{apec}} = 1.82 \times 10^{-5}$ cm^{-5} and $A_{\mathrm{pow}} = 1.22 \times 10^{-6}$ cm^{-5}.

The best-fitting model resulted in an absorbed flux of $f_{\mathrm{X}} = (1.35 \pm 0.35) \times 10^{-14}$ erg s^{-1} cm^{-2} in the 0.4–6.0 keV energy range and corresponds to an intrinsic flux of $F_{\mathrm{X}} = (6.9 \pm 3.3) \times 10^{-14}$ erg s^{-1} cm^{-2}. Taking into account a distance of 0.6 kpc estimated by Santamaría et al. (2019), we calculated an X-ray luminosity of $L_{\mathrm{X}} = (3.0 \pm 1.4) \times 10^{30}$ erg s^{-1}.

Models with varying abundances were also attempted, in particular, models with Ne and Si abundances as free parameters. The Ne abundances resulted in 1.2 times its solar value, whilst the Si abundance converged to values $\sim$3–4 times the solar value. However, these models did not improved considerably the previous fit with a reduced $\chi^2 = 1.16$. Nevertheless, the estimated errors for these two elemental abundances were larger than the actual values. For this, we will keep the model described in the paragraphs above as the best fit to the EPIC-pn spectrum.

---

[2]The normalization parameter is defined in XSPEC as $A = 10^{-14} \int n_{\mathrm{e}} n_{\mathrm{H}} \, \mathrm{d}V/4\pi d^2$, where n_{e} and n_{H} are the electron and hydrogen number densities and d is the distance to the object. The integral is performed over the volume V.
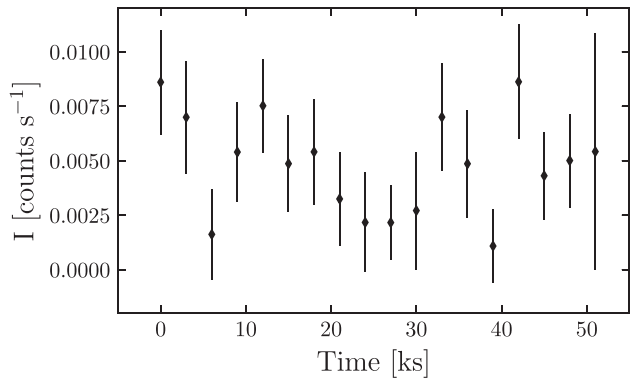
Figure 4. Background-subtracted EPIC-pn light curve in the 0.3–6.0 keV energy range of the central binary system in J210204. Each bin represents 3 ks.
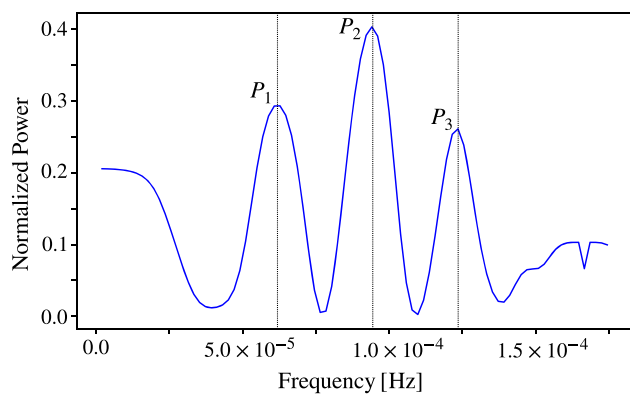

Figure 5. Normalized power spectrum of the light curve presented in Fig. 4. The three peaks marked with dotted lines correspond to frequencies of $(6.2 \pm 0.9) \times 10^{-5}$ Hz, $9.4 \pm 0.4 \times 10^{-5}$ Hz, and $(1.2 \pm 0.7) \times 10^{-4}$ Hz that correspond to periods of $P_1 = 4.5 \pm 0.6$ h, $P_2 = 2.9 \pm 0.2$ h, and $P_3 = 2.3 \pm 0.7$ h, respectively.

To assess the possible X-ray variability of the binary system of J210204, we extracted background-subtracted light curves in the 0.3–6.0, 0.4–2.0, and 1.5–6.0 keV energy ranges. The three light curves are very similar and, thus, we only show that of the EPIC-pn corresponding to the 0.3–6.0 keV energy range in Fig. 4. We used the PYASTRONOMYLomb–Scargle routine to produce a periodogram and calculate the most possible period of variation. This procedure suggests a period of 10.7 ± 0.6 ks ($=2.9 \pm 0.2$ h) for the 0.3–6.0 and 0.4–2.0 keV light curves, and a period of 11.1 ± 0.7 ks ($=3.1 \pm 0.2$ h) for the light curve in the 1.5–6.0 keV range, i.e. the periods in the different energy bands are consistent within their uncertainties. We note that each periodogram exhibited the presence of other two secondary components. We illustrate this in Fig. 5 where we show the normalized power spectrum obtained for the light curve presented in Fig. 4. This periodogram has three main peaks at frequencies $\omega_1 = (6.2 \pm 0.9) \times 10^{-5}$ Hz, $\omega_2 = (9.4 \pm 0.4) \times 10^{-5}$ Hz, and $\omega_3 = (1.2 \pm 0.7) \times 10^{-4}$ Hz. These correspond to periods of $P_1 = 4.5 \pm 0.6$ h, $P_2 = 2.9 \pm 0.2$ h, and $P_3 = 2.3 \pm 0.7$ h, respectively. P_2 is the one described above while P_1 is consistent with that estimated from optical observations of the progenitor system of J210204 of 4.26 ± 0.01 h (see Guerrero et al. 2018).

As shown in the previous section, no extended X-ray emission is detected with the current EPIC observations. In order to estimate

upper limits to the X-ray flux and luminosity of the possible hot bubble in J210204, we extracted a background-subtracted spectrum of a region encompassing that of the nebular emission, excising the contribution from point sources. We estimated a 3σ upper limit to the EPIC-pn count rate in the 0.3–6.0 keV of 0.54 counts ks^{-1}. Using the count rate simulator PIMMS[3] version 4.10, assuming a plasma temperature for the hot bubble of $T = 2 \times 10^6$ K and adopting the $N_H = 8 \times 10^{21}$ cm^{-2} as obtained for the spectral fit of the progenitor system of J210204, we estimated an absorbed flux of $f_{X, DIFF} \lesssim 2.1 \times 10^{-16}$ erg s^{-1} cm^{-2}. This corresponds to an intrinsic flux of $F_{X, DIFF} \lesssim 2.5 \times 10^{-14}$ erg s^{-1} cm^{-2} and an upper limit to the X-ray luminosity of $L_{X, DIFF} \lesssim 1.1 \times 10^{30}$ erg s^{-1}.

4 DISCUSSION

Our best-fitting model to the EPIC-pn spectrum of the progenitor system of J210204 suggests the presence of a thermal component with a temperature of $T_X \approx (6.4 \pm 3.1) \times 10^6$ K. Interestingly, the second component is best described by a power law with a spectral index of $\Gamma = 1.0$, suggesting the presence of non-thermal emission and, thus, a possible IP origin for this stellar system. We note that the number of IP systems in the Galaxy is expected to be large, contributing importantly to the Galactic X-ray properties (Revnivtsev et al. 2009; Warwick, Pérez-Ramírez & Byckling 2011; Warwick, Byckling & Pérez-Ramírez 2014), but not many have been confirmed in the literature.[4] Thus, the characterization of such systems as possible IPs is crucial.

The plasma temperature of the progenitor star of J210204 is very similar to that estimated for other IPs with very similar spectra with dominant emission around 1.0 keV and emission lines above 2 keV (see Worpel et al. 2020, and references therein). We note that although the X-ray emission from IPs is expected to have X-ray luminosities in excess to 10^{32} erg s^{-1} (Patterson 1994), the progenitor system of J210204 has a luminosity of 10^{30} erg s^{-1}, i.e. it is underluminous as the iconic DQ Her (see the recently characterized cases presented in Nucita et al. 2020, 2021, and references therein).

Although the resultant light curves of the EPIC observations of the progenitor system of J210204 do not have an excellent quality, we were able to perform time series analysis. The power spectrum presented in Fig. 5 exhibits three main components. The frequency peak ω_1 implies a period of 4.5 ± 0.6 h, which is very similar to that estimated by Guerrero et al. (2018) using optical observations. Thus, this is very likely to be the orbital period P_{orbit}. If this system is indeed an IP, the dominant frequency ω_2 with a period of $P_2 = 2.9 \pm 0.2$ h could be attributed to the orbital spin of the WD component in the system (P_{spin}). We tried to assess the origin of the third component ω_3 and it seems to follow the relation

$$\omega_3 = \frac{2}{P_{spin}} - \frac{1}{P_{orbit}}, \tag{1}$$

which has been discussed thoroughly in the theoretical calculations of X-ray power spectra presented by Wynn & King (1992). These authors suggested that such frequency could be used an indicator of discless accretion mechanisms, but this seems to depend on different parameters used for the emission model. We reckon, however, that our light curves and periodograms do not have sufficient quality to

further discuss the origin of the accretion on to the progenitor system of J210204. Indeed, broad peaks can appear in the power spectrum as the result of the combination of several components in low-quality X-ray light curves (e.g. see fig. 8 in Wang et al. 2020).

4.1 On the lack of extended X-ray emission

J210204 has a complex nova shell structure, unlike the ellipsoidal shell commonly observed around classical novae (see e.g. Santamaría et al. 2020), but it shares stark similarities to the nova shell around AT Cnc (Shara et al. 2012). The morphological similarities between these two novae suggest that their asymmetries are not produced by interactions with the ISM, but due to the conditions of the explosion itself.

Departures from symmetry might be attributed to the interaction of the ejecta with the companion star and material in the orbital plane of the binary system, but simulations presented in Orlando et al. (2017) show that material is mostly collimated in polar directions of the orbital plane. The same group predicted the evolution of the X-ray luminosity for similar numerical simulations (Orlando, Drake & Laming 2009). They predicted that the total X-ray flux in their simulations achieves a maximum of $\sim 10^{-9}$ erg s^{-1} cm^{-2} after the fourth day of the explosion and then decays as $\sim t^{-1.2}$ mainly due to radiative cooling. Assuming that such evolution of the X-ray flux is valid for J210204, their model predicts an X-ray flux of (1.0–2.5) $\times$ 10^{-14} erg s^{-1} cm^{-2} at the age of 130–170 yr suggested by Santamaría et al. (2020) for J210204, very similar to the upper limit estimated here using *XMM–Newton* EPIC-pn observations. Nevertheless, we would like to remark that different parameters included in the simulations (e.g. E_0 and M_{ej}) could produce a range of X-ray properties (e.g. Orlando & Drake 2012).

However complex the role of the different parameters explored in the simulations discussed above, all of them produce ellipsoidal morphologies (see also Walder, Folini & Shore 2008), which is not the case of J210204 and AT Cnc. The fact that the ejecta of these two novae appear to expand towards one side is suggestive of an explosion that originated from a specific location of the WD surface, i.e. the ejecta is not only axisymmetric, but also asymmetric. Future simulations adopting such scenario might be explored in the future to explain the morphologies of J210204 and AT Cnc.

5 SUMMARY

We presented the analysis of *XMM–Newton* observations of the nova shell IPHASX J210204.7+471015 (J210204). Our EPIC observations detected X-ray emission from the central binary star with properties that are very similar to the so-called IPs: a dominant plasma temperature with temperature of $T_X = (6.4 \pm 3.1) \times 10^6$ K with a power-law component, signature of non-thermal X-ray emission. Its luminosity, $L_X = 10^{30}$ erg s^{-1}, is below the expected value for the X-ray emission from IPs of 10^{32}–10^{34} erg s^{-1}, but consistent with that of DQ Her and other underluminous IPs.

We used time series analysis of the EPIC observations and obtained three dominant frequencies to the power spectrum. The peak with period 4.5 ± 0.6 h seems to correspond to the orbital period of the system as observed at optical wavelengths (e.g. Guerrero et al. 2018). The dominant component to the periodogram corresponds to a period of 2.9 ± 0.2 h very likely related to the spin of the WD. Future deeper X-ray observations are necessary to assess the presence of the dominant components in the power spectrum.

We used the ESAS tasks to search for extended X-ray emission within J210204 as signature of the presence of an adiabatically

shocked hot bubble without success. We estimated an upper limit of the flux and luminosity of the X-ray emission of $F_{X, DIFF} \lesssim 2.5 \times 10^{-14}$ erg s^{-1} and $L_{X, DIFF} \lesssim 1.1 \times 10^{30}$ erg s^{-1}, respectively. This flux is very similar to that estimated from numerical simulations presented in the literature in which the explosion generates an ellipsoidal nova shell. However, due to the remarkable morphology of J210204, we suggest that the explosion might have not occurred isotropically at the boundary of the WD, but it would be rather asymmetric arising from a specific region of the WD. Such claim will have to be put to test with future numerical simulations that will also serve to explain the similar morphology of AT Cnc.

DATA AVAILABILITY

The data underlying this paper are available in the paper. The reduced observations files will be shared on reasonable request to the corresponding author.

REFERENCES

Arnaud K. A., 1996, in Jacoby G. H., Barnes J., eds, ASP Conf. Ser. Vol. 101, Astronomical Data Analysis Software and Systems V. Astron. Soc. Pac., San Francisco, p. 17
Balman Ş., 2005, ApJ, 627, 933
Balman Ş., 2014, A&A, 572, A114
Balman Ş., Küpcü-Yoldaş A., 2004, in Vrielmann S., Meech K. J., eds, IAU Colloq. 190, Magnetic Cataclysmic Variables. Cambridge Univ. Press, Cambridge, p. 172
Balman Ş., Ögelman H. B., 1999, ApJ, 518, L111
Barentsen G. et al., 2014, MNRAS, 444, 3230
Baskill D. S., Wheatley P. J., Osborne J. P., 2005, MNRAS, 357, 626
Bode M. F., 2010, Astron. Nachr., 331, 160
Della Valle M., Izzo L., 2020, A&AR, 28, 3
Drew J. E. et al., 2005, MNRAS, 362, 753
Dyson J. E., Williams D. A., 1997, The Physics of the Interstellar Medium, 2nd edn. IoP Publishing, Bristol
Eracleous M., Halpern J., Patterson J., 1991, ApJ, 382, 290
Gallagher J. S., Starrfield S., 1978, ARA&A, 16, 171
Güdel M., Briggs K. R., Montmerle T., Audard M., Rebull L., Skinner S. L., 2008, Science, 319, 309
Guerrero M. A. et al., 2018, ApJ, 857, 80
Hernanz M., Sala G., 2002, Science, 298, 393
Hernanz M., Sala G., 2010, Astron. Nachr., 331, 169

Kuntz K. D., Snowden S. L., 2008, A&A, 478, 575

Luna G. J. M., Montez R., Sokoloski J. L., Mukai K., Kastner J. H., 2009, ApJ, 707, 1168

Mukai K., Still M., Ringwald F. A., 2003, ApJ, 594, 428

Nucita A. A., De Paolis F., Strafella F., Licchelli D., 2020, MNRAS, 498, 2688

Nucita A. A., De Paolis F., Licchelli D., Strafella F., Ingrosso G., Maiorano M., 2021, ApJ, 906, 134

Orlando S., Drake J. J., 2012, MNRAS, 419, 2329

Orlando S., Drake J. J., Laming J. M., 2009, A&A, 493, 1049

Orlando S., Drake J. J., Miceli M., 2017, MNRAS, 464, 5003

Patterson J., 1994, PASP, 106, 209

Revnivtsev M., Sazonov S., Churazov E., Forman W., Vikhlinin A., Sunyaev R., 2009, Nature, 458, 1142

Sabin L. et al., 2014, MNRAS, 443, 3388

Sala G., Ness J. U., Hernanz M., Greiner J., 2017, A&A, 601, A93

Santamaría E., Guerrero M. A., Ramos-Larios G., Sabin L., Vázquez R., Gómez-Muñoz M. A., Toalá J. A., 2019, MNRAS, 483, 3773

Santamaría E., Guerrero M. A., Ramos-Larios G., Toalá J. A., Sabin L., Rubio G., Quino-Mendoza J. A., 2020, ApJ, 892, 60

Shara M. M., Mizusawa T., Wehinger P., Zurek D., Martin C. D., Neill J. D., Forster K., Seibert M., 2012, ApJ, 758, 121

Singh K. P., Girish V., Pavana M., Ness J.-U., Anupama G. C., Orio M., 2021, MNRAS, 501, 36

Snowden S. L., Collier M. R., Kuntz K. D., 2004, ApJ, 610, 1182

Snowden S. L., Mushotzky R. F., Kuntz K. D., Davis D. S., 2008, A&A, 478, 615

Takei D., Sakamoto T., Drake J. J., 2013, AJ, 145, 18

Takei D., Drake J. J., Yamaguchi H., Slane P., Uchiyama Y., Katsuda S., 2015, ApJ, 801, 92

Toalá J. A., Arthur S. J., 2018, MNRAS, 478, 1218

Toalá J. A., Guerrero M. A., Santamaría E., Ramos-Larios G., Sabin L., 2020, MNRAS, 495, 4372

Vaytet N. M. H., O'Brien T. J., Rushton A. P., 2007, MNRAS, 380, 175

Walder R., Folini D., Shore S. N., 2008, A&A, 484, L9

Wang Q., Qian S., Han Z., Fang X., Zang L., Liu W., 2020, ApJ, 892, 38

Warwick R. S., Pérez-Ramírez D., Byckling K., 2011, MNRAS, 413, 595

Warwick R. S., Byckling K., Pérez-Ramírez D., 2014, MNRAS, 438, 2967

Wilms J., Allen A., McCray R., 2000, ApJ, 542, 914

Worpel H., Schwope A. D., Traulsen I., Mukai K., Ok S., 2020, A&A, 639, A17

Wynn G. A., King A. R., 1992, MNRAS, 255, 83

Yuasa T., Hayashi T., Ishida M., 2016, MNRAS, 459, 779

This paper has been typeset from a TEX/LATEX file prepared by the author.